Validation of ASTER GDEM for the Area of Greece

N. Chrysoulakis, M. Abrams, Y. Kamarianakis, and M. Stanislawski

Abstract

The ASTER (Advanced Spaceborne Thermal Emission and Reflection Radiometer) Global Digital Elevation Model (GDEM), which was released in June 2009, provides elevation data for over 99 percent of Earth's land area. GDEM was found to contain significant anomalies mainly caused by residual clouds in the ASTER scenes, or by the algorithm used to generate the final GDEM from the variable number of individual DEMs. In this paper, the GDEM, for the whole area of Greece was validated by comparing it with reference DEMs with higher resolution derived either from aerial stereo imagery, or from ASTER raw data analysis; as well as with elevation values provided by a number of Geodetic Control Points (GCP) and GPS measurements. The vertical accuracy (at 95 percent confidence) was calculated to be more than 30 m (RMSE = 16.01 m) when compared to the GCPs, whereas the vertical accuracy was calculated around 20 m (RMSE = 11.08 m) when compared with the GPS derived elevations. It can be therefore stated that the current version of ASTER GDEM overall does not meet its pre-production estimated vertical accuracy of 20 m at 95 percent confidence over Greece, however, it can be used in several applications, such as topographic analysis, hydrological and geomorphological modeling, landscape visualization, and energy balance studies.

Introduction

Geo-scientific applications that use georeferenced cartographic/geospatial data require accurate knowledge and visualization of the topography of the Earth's surface. Digital Elevation Models (DEMs), as digital representations of the Earth's topographic relief, provide the basis for many geographic applications such as topographic analysis, hydrological or geomorphological modeling, or landscape visualization. Topographic attributes, such as slope, aspect, or curvature, can be computed over the grid structure of a DEM in a straightforward manner (Ackermann, 1994; Chrysoulakis *et al.*, 2003 and 2004) and can be subsequently used for geometric, radiometric and atmospheric corrections of satellite data (Chrysoulakis *et al.*, 2010). The production of geocoded, ortho-rectified raster images, a necessity for incorporating image data in a Geographic Information Systems (GIS) database, also requires elevation data in the form of DEMs (Toutin, 2008). However, the general ability of the DEM to represent the topography depends on both the roughness of the true surface and the resolution of the DEM. Namely, since terrain contains variations on many scales, and different uses of terrain models require different accuracy, the scale imposed by the DEM resolution affects the topographic parameters (Quattrochi and Goodchild, 1997). Relying on the observation that relief conserves the same statistical characteristics over a wide range of scales, several DEM characterization techniques have been developed that perform a multi-scale analysis of the elevation data (Grazzini and Chrysoulakis, 2005).

DEM generation has become an important part of international research in the last ten years as a result of both the existence of many satellite sensors that can provide stereo imagery and the development of new DEM extraction algorithms (Welch *et al.*, 1998; Toutin *et al.*, 2001; Zhen *et al.*, 2001; Lee *et al.*, 2003; Toutin, 2001, 2004, and 2008). For the production of DEMs from optical satellite data, the respective satellite sensors must have stereo coverage capabilities. Two methods have been proposed to obtain stereoscopy with images from satellite scanners (Toutin, 2001): the along-track stereoscopy with images from the same orbit using fore and aft images, and the across-track stereoscopy from two different orbits. The former method is used in ASTER (Advanced Spaceborne Thermal Emission and Reflection Radiometer) imagery. The ASTER Visible - Near Infrared (VNIR) subsystem consists of two telescopes: one nadir looking with a three band detector (Channels 1, 2, and 3N) and the other backward looking (27.7° off-nadir) with a single band detector (Fujisada, 1994; Abrams, 2000). The data products provided by the ASTER have been summarized by Yamaguchi *et al.* (1998). The ASTER method (along-track stereo acquisition using a nadir and a backward-looking telescope) gives a strong advantage in terms of radiometric variations (because of its near simultaneous nadir and backward acquisitions) versus the multi-date stereo data acquisition with across-track stereo, which can then compensate for its weaker stereo geometry (base to height ratio of 0.6). The viability of stereo correlation for parallax difference from digital stereoscopic data has been described and evaluated in previous studies (Ackermann,

N. Chrysoulakis and M. Stanislawski are with the Foundation for Research and Technology - Hellas, Institute of Applied and Computational Mathematics, N. Plastira 100, Vassilika Vouton, P.O. Box 1385, 71110 Heraklion, Crete, Greece (zedd2@iacm.forth.gr).

M. Abrams is with the Jet Propulsion Laboratory, California Institute of Technology, MS 183–501, 4800 Oak Grove Drive, Pasadena, CA 91109.

Y. Kamarianakis is at Cornell University, School of Civil & Environmental Engineering, 462 Hollister Hall, Ithaca, NY 14853.

Photogrammetric Engineering & Remote Sensing
Vol. 77, No. 2, February 2011, pp. 157–165.

0099-1112/11/7702–0157/$3.00/0

1994; Bolstad and Stowe, 1994; Hohle, 1996; Al-Rousan and Petrie, 1998; Lang and Welch, 1999; Toutin, 2001 and 2004). The basic characteristics of stereoscopy and its application to the ASTER system for DEM generation have been recently reviewed by Toutin (2008). He addressed the methods, algorithms and commercial software to extract absolute or relative elevation. Furthermore, Toutin (2008) assessed their performance using results from various organizations and discussed the use of the DEMs derived from ASTER stereo pairs in different applications.

Many efforts to assemble global elevation datasets have been undertaken in the past few decades. In 1986, SPOT was the first satellite to provide stereoscopic images that allowed extraction of DEMs over large areas of the Earth's surface. For the first time, the scientific community was able to extract three-dimensional data over areas of interest that were still inaccessible before the launch of SPOT (Al-Rousan and Petrie, 1998). Since that time, various analogue or digital sensors in the visible spectrum have been flown, providing users with spatial data for extracting and interpreting three-dimensional information on the Earth's surface (Nikolakopoulos *et al.*, 2006). The SRTM mission (Werner, 2001; Rosen *et al.*, 2001; Farr *et al.*, 2007) was the first mission using spaceborne single-pass interferometric Synthetic Aperture Radar (SAR). The SRTM DEM products are being distributed mainly under two forms; these are the SRTM-1 and SRTM-3, with spatial resolution of 1 arc-second (around 30 m) and 3 arc-seconds (around 90 m), respectively. The first is available only for the United States, while the latter is available for the rest of the globe. The most recent global DEM source is the ASTER Global Digital Elevation Model (GDEM) which was released by Japan's Ministry of Economy, Trade and Industry (METI) and United States National Aeronautics and Space Administration (NASA) on 29 June 2009. GDEM is a global DEM generated using ASTER data, with 30 m posting. At the November 2007 GEO Ministerial Summit, NASA and METI were invited by GEO to contribute this global DEM to GEOSS (Global Earth Observation System of Systems), and both countries accepted the invitation. The ASTER GDEM was created by stereo-correlating the entire ASTER archive, stacking and averaging the individual DEMs, cloud screening, filling voids or holes using SRTM-3 arc-second data, and validating the GDEM against higher resolution DEMs worldwide (Abrams *et al.*, 2010). GDEM was found to contain significant anomalies, which will affect its usefulness for certain user applications. Given that the water bodies can be effectively masked in ASTER imagery, there are two primary sources of these anomalies. One is residual clouds in the ASTER scenes used to generate the GDEM, and the other is the algorithm used to generate the final GDEM from individual ASTER DEMs available to contribute to the final elevation value for any given pixel (GDEM Validation Team, 2009).

Global elevation datasets are inevitably subject to errors, mainly due to the methodology followed to extract elevation information and the various processing steps the models have undergone (e.g., interpolation). Extensive and systematic evaluation of such datasets is difficult due to lack of substantial ground truthing. Error in elevation data is widely recognized to comprise mainly two components: the horizontal, often referred as positional accuracy, and the vertical component. However, horizontal and vertical accuracy generally cannot be separated; the error may be due to an incorrect elevation value at the correct location, or a correct elevation for an incorrect location or some combination of these. Fisher and Tate (2006) provided a detailed description of causes and consequences of error in DEMs. For stereo systems, elevation accuracy is generally of the order of the system instantaneous field of view, or approximately the pixel spacing, also taking into account the Base-to-Height ratio (B/H) (Toutin, 2008). The theoretical accuracy of ASTER DEMs is governed by the accuracy of the control data, the B/H and the image matching. Since an error of ± 0.5 to 1 pixel or better for the parallax measurements in the automated matching process has been achieved with different datasets from other sensors, the potential relative accuracy for the elevation with the ASTER stereo data (B/H = 0.6, pixel spacing of 15 m) could be of the order of 12 m to 25 m or better (Welch *et al.*, 1998), depending on the type of terrain. In addition, the accuracy of the DEM will also be dependent on the geometric parameter calibration, as well as the accuracy of the ephemeris and attitude data for computing the direct georeferencing (Toutin, 2008).

A detailed study compared Conterminous United States (CONUS) GDEM data (934 GDEM tiles) to the United States Geological Survey (USGS) National Elevation Dataset (NED) and calculated an overall vertical Root Mean Square Error (RMSE) of 10.87 m (GDEM Validation Team, 2009). When compared with more than 13,000 GCPs from CONUS, the RMSE dropped to 9.37 meters (Abrams *et al.*, 2010). These values convert, respectively, to vertical errors of just over and just under the estimated ASTER GDEM vertical error of 20 meters at 95 percent confidence. Studies around the globe confirmed that detailed vertical accuracy results obtained for CONUS can, in general, be extrapolated with confidence to other parts of the world. RMSEs for individual tiles vary from much better than the average CONUS results to considerably worse, as numerous factors affect local GDEM accuracy. However, the overall accuracy of the ASTER GDEM, on a global basis, can be taken to be approximately 20 meters at 95 percent confidence (GDEM Validation Team, 2009).

In this paper, the ASTER GDEM product for the whole area of Greece is validated using Geodetic Control Points (GCPs) and GPS measurements as checkpoints. Moreover, the GDEM for a rural area in Crete (Heraklion), as well as for an urban area (Athens), are compared with the ASTER DEMs which were produced in the framework of the REALDEMS project (Chrysoulakis *et al.*, 2004). REALDEMS was a joint effort of Foundation for Research and technology; Hellas (FORTH), the Jet Propulsion Laboratory (JPL), the University of the Aegean, and Plano S. A., aimed at producing DEM and land-cover maps for some of the Greek islands. The REALDEMS methodology was extended by FORTH after the completion of the project to develop a DEM for the Prefecture of Attica which includes Athens, the capital of Greece. Detailed information about these reference ASTER DEMs is given by Chrysoulakis *et al.* (2004), Chrysoulakis and Abrams (2005), and Nikolakopoulos *et al.* (2006). Finally, the GDEM for the Northern part of Rhodes Island is compared with a high-resolution DEM (post-spacing of 5 m) derived from aerial stereo images in the framework of the European project TRANSFER (Chrysoulakis *et al.*, 2008) aimed at tsunami hazard and risk assessment and the identification of the best strategies for reduction of tsunami risk.

Data and Methodology

GDEM was evaluated against checkpoints that were evenly distributed over the Greek territory. Furthermore GDEM was compared against reference DEMs which were produced in REALDEMS and TRANSFER projects, using ASTER stereo pairs and aerial stereo imagery, respectively. Three areas (Athens, Heraklion, and Rhodes) with a complex physiography (urban areas included), an extensive drainage network, and elevations that range from 0 to more than 2,100 m were selected.

The GDEM Datasets

The ASTER GDEM is being distributed by METI and NASA through the Earth Remote Sensing Data Analysis Center (ERSDAC, 2009) and the NASA Land Processes Distributed Active Archive Center (LP DAAC, 2009) at no charge to

users worldwide as a contribution to GEOSS. GDEM was produced by automated processing of the entire 1.5-million scene ASTER archive, including stereo-correlation to produce 1,264,118 individual scene-based ASTER DEMs, cloud masking to remove cloudy pixels, stacking all scene-based DEMs, removing residual bad values and outliers, averaging selected data to create final pixel values, and then correcting residual anomalies before partitioning the data into 1°-by-1° tiles. It covers land surfaces between 83°N and 83°S with estimated accuracies of 20 meters at 95 percent confidence for vertical data and 30 meters at 95 percent confidence for horizontal data. The ASTER GDEM is in GEOTIFF format with geographic (latitude/longitude) coordinates and a 1 arc-second grid. For each 1°-by-1° tile; two files are delivered: (a) a DEM data file, and (b) a quality assessment (QA) file which shows the number of scene-based DEMs contributing to the final DEM value at each post or the location of data anomalies that have been corrected, and the data source used for the correction. Fifty ASTER GDEM tiles that cover the whole area of Greece were downloaded from ERSDAC and a mosaic DEM that corresponds to the above area was generated. It should be noted that a part that covers Southern Greece (southern area of Crete island) is missing; this area corresponds to tiles 34N-25E and 34N-26E which are not included in the GDEM dataset. A DEM for this area has been produced in REALDEMS (Chrysoulakis *et al.*, 2004), and it is available at no cost to the scientific community.

The Reference DEMs and the Checkpoints

Three reference DEMs and a set of checkpoints were used in the validation study:

- A DEM corresponding to an urban area. This DEM was selected as a part of the city of Athens (Figure 1); it was produced by combining ASTER stereo pairs and ancillary data (GPS measurements, road networks, etc.) in the framework of REALDEMS. The spatial resolution of this DEM was 15 m × 15 m in Hellenic Geodetic Reference System 87 (HGRS87), and its vertical accuracy was better than 20 m (Chrysoulakis *et al.*, 2004; Nikolakopoulos *et al.*, 2006). It was then resampled to 30 m × 30 m and transformed to Geographic WGS84/EGM96 (World Geodetic System 1984/ Earth Gravitational Model 1996).
- A DEM that corresponds to a rural area. This DEM which covers a part of central Crete and includes the Northern part of the Prefecture of Heraklion and the Plateau of Lassithi (Figure 1) was also produced in the framework of REALDEMS. The spatial resolution of this DEM was 15 m × 15 m in HGRS87, and its vertical accuracy was better than 20 m (Chrysoulakis *et al.*, 2004; Nikolakopoulos *et al.*, 2006). It was also resampled to 30 m × 30 m and transformed to Geographic WGS84/EGM96.
- A very high resolution DEM for the area of the Municipality of Rhodes (Figure 1). This DEM was derived by aerial stereo imagery and used for inundation mapping in the framework of the TRANSFER project. The spatial resolution of this DEM was 5 m × 5 m in HGRS87, and its vertical accuracy was better than 2 m (Chrysoulakis *et al.*, 2008). It was also resampled to 30 m × 30 m and transformed to Geographic WGS84/EGM96.
- The checkpoints that were used in this study came from two different sources.
- The first checkpoints dataset was a subset from the GCPs of the National Trigonometric Network for Greece provided by the Hellenic Military Geographical Service (HMGS, 2009). More than 5,000 checkpoints in HGRS87 evenly distributed over the Greek territory were used (Figure 1). The accuracy of their orthometric heights was better than 1 m, referred to the Earth's equipotential surface that coincides with the mean sea level at the Hellenic Vertical Datum fundamental tide-gauge reference station (Kotsakis *et al.*, 2008). These points were available from 1:5000 topographic maps and were transformed to Geographic WGS84/EGM96.
- The second checkpoints dataset consisted of GPS positions acquired in Central Crete in the framework of REALDEMS projects (Chrysoulakis *et al.*, 2004). These GPS measurements were differentially corrected using the GPS base station of FORTH. The Earth Gravitational Model EGM08, which has been recently released by the U.S. National Geospatial-Intelligence Agency (Pavlis *et al.*, 2008) was used to correct these checkpoints for the geoid separation for Greece. The EGM08 raster data set of 2.5-minute geoid undulation values (Pavlis *et al.*, 2008) was used.

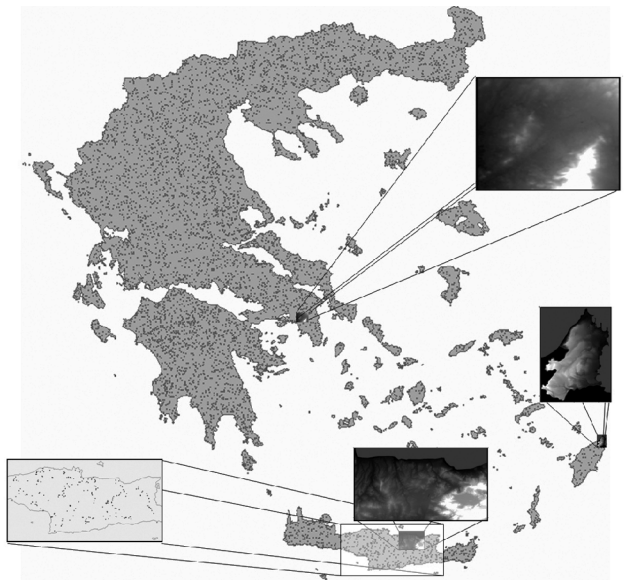

Figure 1. The study area and the locations of the three DEMs (Athens in the upper right rectangle, Heraklion in the lower right rectangle and Rhodes is middle right rectangle). The spatial distribution of checkpoints within the study area is also shown; the GCPs are depicted as dots in grey background, whereas the locations of the GPS measurements are depicted as dots in white background (rectangle on the left).

The Comparison Methodology

To compare the elevation distributions derived from GDEM with the three reference DEMs and the checkpoints, several descriptive statistical measures were employed, among them skewness and kurtosis (Nikolakopoulos *et al.*, 2006). The elevation of each GDEM post was compared with the respective reference elevation and the Root Mean Square Error (RMSE) was calculated directly from raster data. Mean Absolute Error (MAE) and Median Absolute Error (MedAE) are also displayed; the latter is robust to outliers and a better estimator of the central tendency of absolute error when it is asymmetrically distributed. RMSE, MAE, and MedAE are global measures of accuracy. To provide an indication of the spatial distribution of error at local level, dot maps that present the magnitude of error in the neighborhood of each checkpoint were developed and an example of such a map is shown in the next section (Figure 9).

The RMSE was calculated as described in Chrysoulakis *et al.* (2004) and Hadjimitsis *et al.* (2009): Let $Z_{CP}(i)$ denote the elevation of checkpoint i. To overcome the random error caused by any horizontal offsets associated with each GDEM value, a buffer zone was created around each checkpoint; these zones were circles with a radius of 30 m. The set of these

zones was superimposed on GDEM and the spatial average of the GDEM elevation in each zone, denoted by $Z_{GDEM}(i)$ was calculated. For each zone i, the calculated elevation value $Z_{GDEM}(i)$ was compared with $Z_{CP}(i)$ of the respective checkpoint. Consequently, the RMSE was calculated as:

$$RMSE = \sqrt{\frac{1}{n}\sum_{i=1}^{n}\delta z_i^2} \quad (2)$$

where, δz_i is the $Z_{GDEM}(i)$ - $Z_{CP}(i)$ differences and n is the number of checkpoints. Bias was analogously estimated using the above buffer zones.

To quantify the strength of linear association between GDEM and reference DEMs, Pearson's and Spearman's correlation coefficients were calculated. Pearson's product-moment correlation is a parametric measure of a linear relationship between two variables; it is the most widely used correlation measure and its statistical significance is evaluated on the basis of distributional assumptions on the examined pair of variables. On the other hand, Spearman's rank-order correlation statistic uses the ranks of the data values, and the test of its statistical significance is free from distributional assumptions. Preliminary analysis indicated that there was significant spatial correlation in the GDEM and reference DEMs datasets, which inflated the corresponding correlation coefficients. For this reason, correlation measures were calculated on sub-samples of GDEM and reference DEMs with a sampling rate that reduced spatial correlation substantially. Based on past variogram analysis (Nikolakopoulos *et al.* 2006), sub-samples with a minimum distance of 50 posts between sample points were selected and correlation coefficients were calculated on these sub-samples. The selected sampling distance allowed for a sample size of 78 sampling points for Athens, 578 sampling points for Heraklion and 34 points for Rhodes, with very low spatial autocorrelation.

Correlation coefficients close to unity imply strong linear associations and subsequently very good fit for equations such as:

$$Z_{GDEM}(i) = \alpha_0 + \beta_0\, Z_{CP}(i) + \varepsilon(i) \text{ or}$$
$$Z_{GDEM}(i) = \alpha_1 + \beta_1\, Z_{ReferenceDEM}(i) + \varepsilon(i)$$

where α_0, α_1, β_0, β_1, are unknown coefficients that need to be estimated while the epsilons represent the random error which should not display large variability. One may rewrite the above equations as:

$$Z_{GDEM}(i) - Z_{CP}(i) = \alpha_0 + (\beta_0 - 1)\, Z_{CP}(i) + \varepsilon(i)$$

and

$$Z_{GDEM}(i) - Z_{ReferenceDEM}(i) = \alpha_1 + (\beta_1 - 1)\, Z_{ReferenceDEM}(i) + \varepsilon(i)$$

Now the coefficients α_0, α_1, β_0, β_1, can be assigned a physical meaning, in the sense that if β_0, β_1 deviate substantially from unity, the data provide strong evidence of elevation dependent bias. If, on the other hand, the null hypothesis that states that the above slopes are equal to unity cannot be rejected, one may quantify the bias of estimated elevations based solely on α_0, α_1. Here, to estimate the coefficients in the above equations, we performed both a (conventional) least squares (LS) procedure and a robust-to-outliers least absolute deviations (LAD) algorithm. Confidence intervals and hypothesis tests on the estimated coefficients are usually based on the hypothesis that epsilons are independent and homoscedastic; that is, their variance is fixed across observations. Since the data provided evidence against the null hypothesis of homoscedastic errors, robust (to heteroscedasticity) confidence intervals for the estimated coefficients were calculated. Confidence intervals for the least squares estimates were based on covariance matrices that were estimated according to the method suggested in MacKinnon and White (1985), whereas heteroscedasticity-robust confidence intervals for LAD estimates were based on the resampling procedure proposed in He and Hu (2002). Hypothesis tests on the coefficients were based on the corresponding confidence intervals.

Results and Discussion

The GDEM for Greece is shown in Figure 2. Catchments and mountainous areas are clearly depicted; the shoreline and the border lines are superimposed. Figure 3 displays histograms and summary statistics for the three examined sub-areas within Greece that were examined. It appears that the distributions derived from GDEM and reference DEMs for each area are similar with regard to symmetry and fat-tailedness, since skewness and kurtosis practically coincide. On the other hand, GDEM elevation observations are slightly less dispersed. The RMSE, MAE, MedAE, as well as the 95 percent quantile of absolute error ($AE_{95\%}$) for Athens, Heraklion, and Rhodes cases are shown in Table 1. In accordance with intuition, the worst performance is achieved in the urban area (Athens case), since man-made features increase the complexity and the roughness of the urban surface and introduce more noise complicating the comparison. The DEMs for all areas display almost perfect linear associations, as shown in Table 2, with slightly weaker correlations for the case of Rhodes.

Ideally, GDEM would display negligible bias, so linear relationships between GDEM and reference DEMs would be represented by equations with estimated slopes very close to unity, estimated intercepts close to zero and small variability for the error terms of the models, however, systematic errors have been reported by Hirt *et al.* (2010). The scatter plots of GDEM versus reference DEMs, for Athens, Heraklion, and Rhodes are shown in Figures 4, 5, and 6, respectively. These scatterplots are again based on sub-samples of GDEM and reference DEMs to avoid the errors introduced by spatial correlation. GDEM overestimated the elevation for Athens and Rhodes, but underestimated it for Heraklion. Estimated (using both LS and LAD) intercepts ($\alpha_{0,LS}$ and $\alpha_{0,LAD}$) and slopes ($\beta_{0,LS}$ and $\beta_{0,LAD}$) and the associated 95 percent confidence intervals are shown

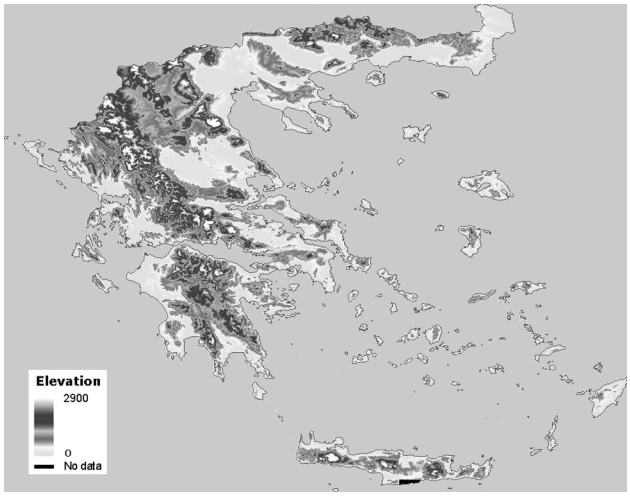

Figure 2. A DEM for Greece that was generated using the GDEM tiles.

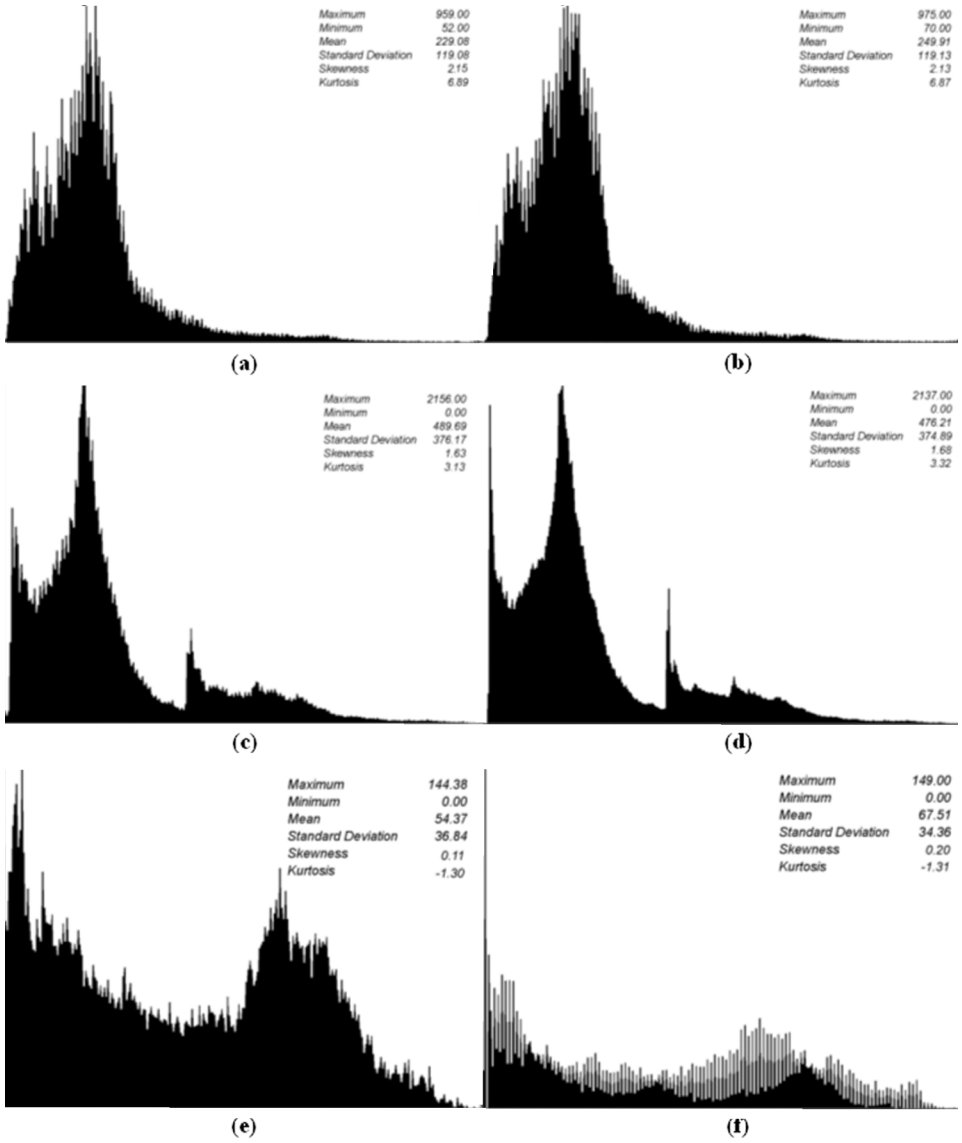

Figure 3. Histograms and the summary statistics for reference DEMs: (a) REALDEMS Athens, (b) GDEM Athens, (c) REALDEMS Heraklion, (d) GDEM Heraklion, (e) TRANSFER Rhodes, and (f) GDEM Rhodes for the three areas examined in this study.

TABLE 1. ACCURACY MEASURES (RMSE, MAE, MEDAE, AND $AE_{95\%}$) FOR ATHENS, HERAKLION, AND RHODES CASES

	RMSE (m)	MAE (m)	MedAE (m)	$AE_{95\%}$ (m)
Athens	21.21	20.85	21.42	26.61
Heraklion	11.93	10.50	10.10	21.09
Rhodes	13.45	12.21	12.18	25.08

TABLE 2. CORRELATION COEFFICIENTS FOR THE ASSOCIATIONS BETWEEN THE THREE REFERENCE DEMS WITH THE RESPECTIVE GDEM PRODUCTS

Area	Pearson's Coefficient (r)	Spearman's Coefficient (ρ)
Athens	0.9994	0.9976
Heraklion	0.9998	0.9996
Rhodes	0.9777	0.9393

in Table 3. The null hypothesis of no elevation dependent bias cannot be rejected for Athens and Rhodes, as in both LS and LAD estimated slopes, unity is included in the 95 percent confidence intervals. On the other hand, statistically significant bias is observed in both cases as zero is not included in the confidence intervals of the corresponding intercepts. Therefore, bias can be estimated using the estimated intercepts, constraining the slope to unity. For Athens, such an estimate for the intercept equals 20.854 with a 95 percent confidence interval given by (19.986, 21.722). The corresponding LAD intercept equals 21.422 with 95 percent confidence interval given by (20.115, 22.729). For Rhodes, the LS estimated intercept, constraining the slope to unity, equals 10.753 with a 95 percent confidence interval given by (6.531, 14.976). The corresponding LAD intercept equals 12.176 with 95 percent

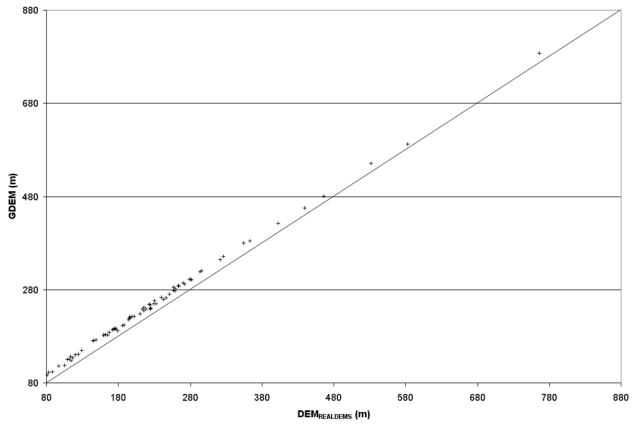

Figure 4. Scatter-plot of GDEM versus REALDEMS elevation sub-sample for the area of Athens. A strong positive correlation ($R^2 = 0.99$) between the GDEM and the reference DEM, as well as an overestimation of GDEM are observed.

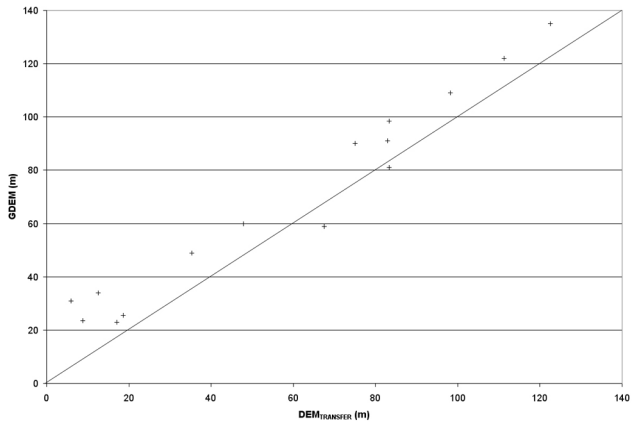

Figure 6. Scatter-plot of GDEM versus TRANSFER elevation sub-sample for the area of Rhodes. A strong positive correlation ($R^2 = 0.96$) between the GDEM and the reference DEM, as well as an overestimation of GDEM are observed.

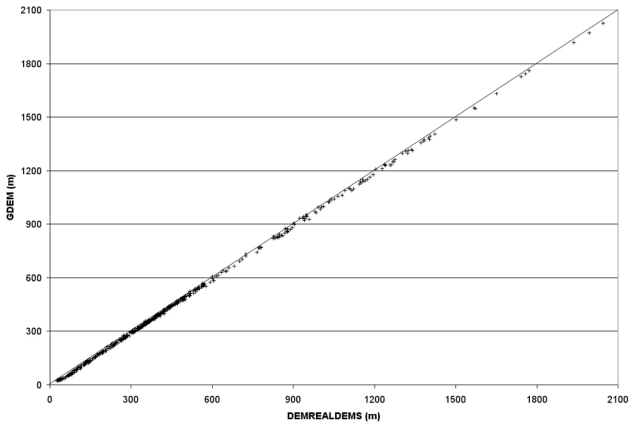

Figure 5. Scatter-plot of GDEM versus REALDEMS elevation sub-sample for the area of Heraklion. A strong positive correlation ($R^2 = 0.99$) between the GDEM and the reference DEM, as well as an underestimation of GDEM are observed.

confidence interval given by (7.701, 16.651). In contrast with the previous cases, confidence intervals for slopes that correspond to the region of Heraklion provide evidence against the null hypothesis of no elevation dependent bias (Table 3).

Very strong correlation was found between the GDEM and the elevation derived from the first checkpoint dataset (GCPs) as can be observed in Figure 7, where a scatter-plot between Z_{GDEM} and Z_{CP} is shown. A RMSE of 16.01 was calculated. The corresponding LS estimated intercept equals 11.016 with a 95 percent confidence interval given by (10.939, 11.073); the LAD intercept differs substantially as it equals 13.371 with an associated confidence interval given by (12.689, 14.052). LS estimated slope was equal to 0.996, and LAD estimated slope was found equal to 0.994 with corresponding confidence intervals given by (0.995, 0.996) and (0.994, 0.995), respectively. As unity is not included in the confidence intervals for slopes, there is evidence of elevation dependent bias.

The above RMSE value is relatively high if compared with the less than 11 m values that were reported for both USA and Japan (GDEM Validation Team, 2009). The following two factors may contribute to the RMSE magnitude:

- The vertical datum conversion during the reprojection of the GCPs from HGRS87 to Geographic (WGS84/EGM96) system.
- The horizontal offset of GDEM, in some cases, was more than one pixel, whereas the horizontal offset of the reference ASTER DEMs was less than 15 m. The reason is that the reference DEMs were used to orthorectify the respective VNIR ASTER channels. Then, the horizontal offset of the multilayer (DEM plus VNIR) map was further corrected using high resolution road network vectors which were overlaid and clearly distinguished in the VNIR image. In this way, the horizontal offset of the reference DEMs was corrected to less than 0.5 pixel RMSE using a 2D polynomial transformation (Hadjimitsis *et al.*, 2009).

TABLE 3. INTERCEPTS, SLOPES, AND ASSOCIATED HETEROSCEDASTICITY; ROBUST 95 PERCENT CONFIDENCE INTERVALS (IN PARENTHESES)

	$\alpha_{0,LS}$	$\alpha_{0,LAD}$	$\beta_{0,LS}$	$\beta_{0,LAD}$
Athens	21.213	21.204	0.998	1.001
	(19.290, 23.136)	(18.198, 24.210)	(0.991, 1.006)	(0.987, 1.014)
Heraklion	−8.760	−9.041	0.997	0.997
	(−9.534, −7.987)	(−10.081, −8.001)	(0.996, 0.999)	(0.995, 0.999)
Rhodes	14.565	15.068	0.934	0.961
	(6.997, 22.131)	(6.462, 29.028)	(0.825, 1.043)	(0.751, 1.172)

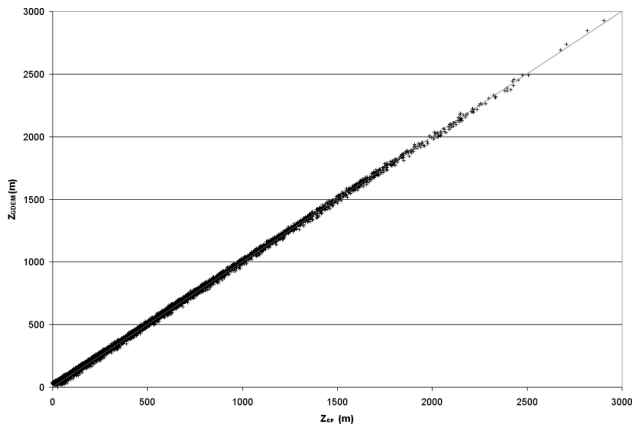

Figure 7. Scatter-plot between Z_{GDEM} and Z_{CP}. An excellent correlation is observed.

The correlation between the GDEM and the elevation derived from the second checkpoint dataset (GPS measurements) was stronger than the correlation between GDEM and GCPs. The GPS derived elevations were converted to orthometric elevations using the EGM08. A RMSE of 11.08 m was calculated. This RMSE value is closer to the respective RMSE values estimated over USA and Japan (GDEM Validation Team, 2009). However, the above comparison was made only for central Crete, because differential GPS measurements were available only for this region, as it was the main validation area of the REALDEMS project (Chrysoulakis and Abrams, 2005).

The RMSE is an aggregated measure of the vertical accuracy of the produced DEM. To assure its accuracy at local level, one may visualize how the difference $Z_{GDEM} - Z_{CP}$ is distributed in space; hence one may depict the magnitude of this difference around each checkpoint. For this purpose a new set of circular buffer zones around each checkpoint was created, however this time the radius of each buffer was equal to 10 times the absolute value of the difference $Z_{GDEM} - Z_{CP}$. A dot map of these buffers over the GDEM reflects how the error is distributed in space. Figure 8 shows the error map produced for tile 39N-21E, which is located in the central part of Greece and corresponds to a mountainous area. The performance of GDEM for this tile is rather good (RMSE = 13.43). The

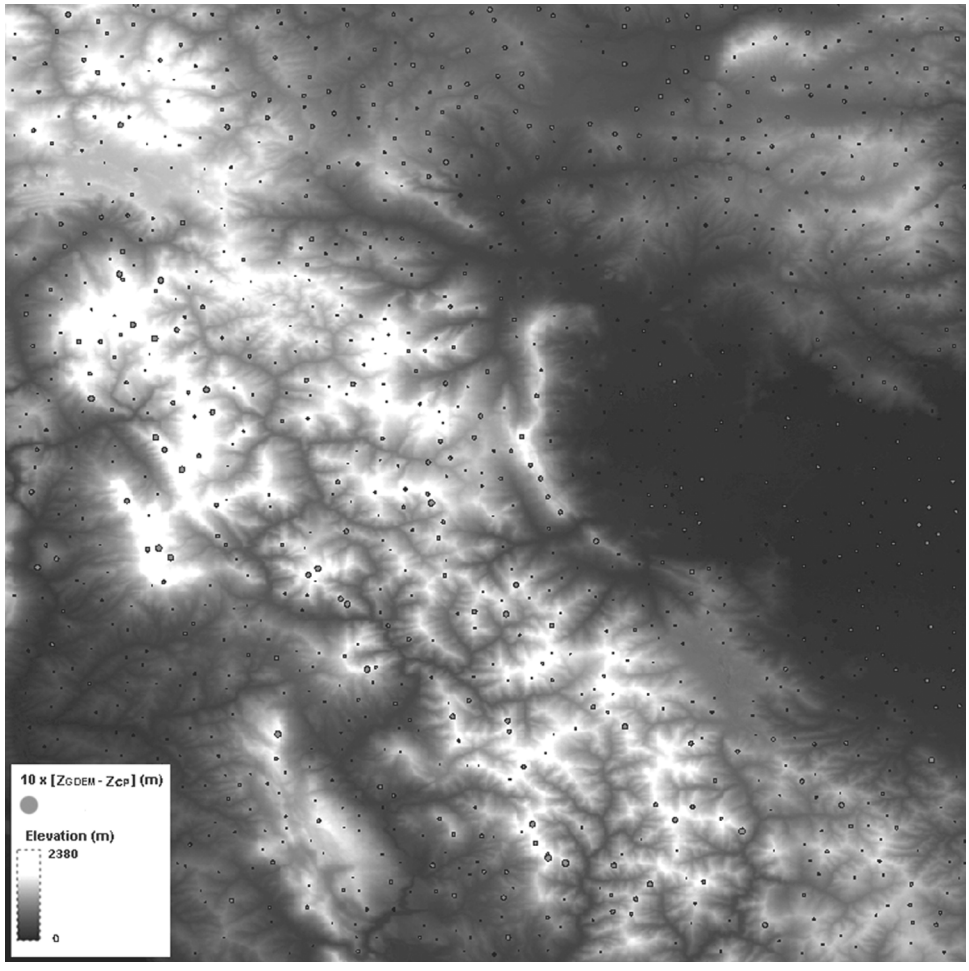

Figure 8. Dot-map presenting the local level performance of GDEM. The radius of each circle is ten times the difference between the GDEM elevation and the elevation of the respective checkpoint. It is obvious that the deviation is higher in areas with high relief.

dots that are shown in Figure 8 represent circles with radius equal to 10 times the Z_{GDEM} - Z_{CP} difference.

Conclusions

Statistical measures were used to estimate GDEM vertical accuracy. The results indicated strong correlation between GDEM and reference DEMs in all cases. Individually, the GDEM and reference DEMs each showed spatial autocorrelation. For this reason, the correlation procedure was repeated using sub-samples of spatially uncorrelated points. The correlation coefficients corresponding to these sub-samples were high in all cases, indicating a strong correlation of the respective datasets. The RMSE values for the GDEM/reference DEM differences were 21.21 m, 11.93 m, and 13.44 m for Athens, Heraklion, and Rhodes areas, respectively. In accordance with intuition, the worst accuracy is achieved in the urban area (Athens case).

The GDEM was compared against the GCPs evenly distributed over the Greek territory, and a RMSE of 16.01 m was calculated, which was higher than the respective RMSEs reported for USA and Japan (GDEM Validation Team, 2009), but it is much less than the RMSE that was reported for SRTM data for the same area (Nikolakopoulos *et al.*, 2006). Finally, the GDEM for the area of Crete was compared against GPS measurements and a RMSE of 11.08 m was calculated, which was slightly better than both the RMSE (12.41 m) that was reported for the same area by Chrysoulakis and Abrams (2005), and the RMSE (19.73 m) that was reported by Hadjimitsis *et al.* (2009) for the area of Cyprus. Given GDEM spacing (30 m), an RMSE of 11.08 m is acceptable, however, it does not meet the published specification of 20 m LE95. The GDEM mosaic covering the whole country was finally reprojected to HGRS87, and it is available at no cost to the Greek scientific community. It can be used as a data product in its own right, as well as to perform 3D orthorectification of different remote sensing images. It is known that 10 to 20 m accurate ASTER DEMs can be used in the generation of Reference Product orthoimages from Ikonos, whose accuracy standard specifies 25 m positional accuracy with a 90 percent level of confidence. The GDEM mosaic is suitable for a large range of environmental and geo-scientific applications including the above mentioned orthorectification procedures.

Acknowledgments

The research leading to these results has received funding from the European Community's Seventh Framework Programme (FP7/2007-2013) under Grant Agreement No. 211345 (BRIDGE Project). Work by Abrams was performed at the Jet Propulsion Laboratory, California Institute of Technology under contract with the National Aeronautics and Space Administration.

References

Abrams, M., B. Bailey, H. Tsu, and M. Hato, 2010. The ASTER Global DEM. *Photogrammetric Engineering & Remote Sensing*, 76(3):344–348.

Abrams, M., 2000. ASTER: Data products for the high spatial resolution imager on NASA's EOS-AM1 platform, *International Journal of Remote Sensing,* 21:847–861.

Ackermann, F., 1994. Digital elevation models - Techniques and application, quality standards, development, *International Archives of Photogrammetry and Remote Sensing*, 30:421–432.

Al-Rousan, N., and G. Petrie, 1998. System calibration, geometric accuracy testing and validation of DEM and orthoimage data extracted from SPOT stereopairs using commercially available image processing systems, *International Archives of Photogrammetry and Remote Sensing*, 32:8–15.

Bolstad, P.V., and T. Stowe, 1994. An evaluation of DEM accuracy: Elevation, slope, and aspect, *Photogrammetric Engineering & Remote Sensing,* 60(12):1327–1332.

Chrysoulakis, N., M. Abrams, H. Feidas, and A. Korei, 2010. Comparison of atmospheric correction methods using ASTER data for the area of Crete, Greece, *International Journal of Remote Sensing* (in press).

Chrysoulakis, N., E. Flouri, E. Diamandakis, V. Dougalis, D.E. Synolakis, and S. Foteinis, 2008. Remote sensing in support of tsunami mitigation planning in the Mediterranean, *Proceedings of the 1st International Conference on Remote Sensing Techniques in Disaster Management and Emergency Response in the Mediterranean Region*, Zadar, Croatia, unpaginated CD-ROM.

Chrysoulakis, N., M. Abrams, H. Feidas, and D. Velianitis, 2004. Analysis of ASTER multispectral stereo imagery to produce DEM and land cover databases for Greek Islands: The REALDEMS project, *Proceedings of e-Environment: Progress and Challenges* (P. Prastacos, U. Cortes, J.L. De Leon, and M. Murillo, editors), pp. 411–424.

Chrysoulakis, N., I. Keramitsoglou, and C. Cartalis, 2003. Hydrologic land cover classification mapping at the local level with the combined use of ASTER multispectral imagery and GPS measurements, *Proceedings of the 10th SPIE International Symposium on Remote Sensing: Remote Sensing for Environmental Monitoring, GIS Applications, and Geology III* (M. Ehlers, editor), pp. 5239, 2003.

Chrysoulakis, N., and M. Abrams, 2005. The use of ASTER imagery in GIS-based watershed analysis at Mediterranean Islands, *Proceedings of the International Workshop for Geomatics for Land and Water management: Achievements and Challenges in the EUROMED Context* (R. Escadafal and M.L. Paracchini, editors), European Commission, Joint Research Centre, EUR 2167 EN. ISBN 92-894-9425-5, pp. 23–34.

ERSDAC, 2009. ASTER GDEM, Earth Remote Sensing Data Analysis Center, URL: *http://www.gdem.aster.ersdac.or.jp/index.jsp* (last date accessed: 20 November 2010).

Farr, T.G, P.A. Rosen, E. Caro, R. Crippen, R. Duren, S. Hensley, M. Kobrick, M. Paller, E. Rodriguez, L. Roth, D. Seal, S. Shaffer, J. Shimada, J. Umland, M. Werner, M. Oskin, D. Burbank, and D. Alsdorf, 2007. The Shuttle Radar Topography Mission, *Reviews of Geophysics*, 45, RG2004, doi:10.1029/2005RG000183.

Fisher, P.F., and N.J. Tate, 2006. Causes and consequences of error in digital elevation models, *Progress in Physical Geography,* 30:467–489.

Fujisada, H., 1994. Overview of ASTER instrument on EOS-AM1 platform, *Proceedings of SPIE*, 2268:14 -36.

GDEM Validation Team, 2009. ASTER Global DEM Validation Summary Report, ASTER GDEM Validation Team: METI/ERSDAC, NASA/LPDAAC/USGS/EROS in cooperation with NGA and other collaborators, URL: *http://asterweb.jpl.nasa.gov/gdem.asp* (last date accessed: 20 November 2010).

Grazzini, J., and N. Chrysoulakis, 2005. Extraction of surface properties from a high accuracy DEM using multiscale remote sensing techniques, *Proceedings of the 19th International Conference: Informatics for Environmental Protection-EnviroInfo2005* (J. Hřebiček and J. Ráček, editors), Masaryk University in Brno, Vol. 1, pp. 352–356.

Hadjimitsis, D., N. Chrysoulakis, A. Retalis, and K. Themistocleous, 2009. Analysis of ASTER multispectral stereo imagery to update DEM and land cover databases for Cyprus island, *Proceedings of the 29th Annual EARSeL Symposium*, 15–18 June, Chania, Greece, unpaginated CD ROM.

He, X., and F. Hu, 2002. Markov Chain Marginal Bootstrap, *Journal of the American Statistical Association*, 97:783–795.

Hirt, C., S. Filmer, and W.E. Feathertone, 2010. Comparison and validation of the recent freely available ASTER GDEM ver1, SRTM ver4.1 and GEODATA DEM-9S ver3 digital elevation models over Australia, *Australian Journal of Earth Sciences*, 57:337–347.

Hohle, J., 1996. Experience with the production of digital orthophotos, *Photogrammetric Engineering & Remote Sensing*, 62:1189–1194

HMGS, 2009. Geodetic Control Points, Hellenic Military Geographical Service, URL: *http://web.gys.gr* (last date accessed: 20 November 2010).

Kotsakis, C., K. Katsambalos, D. Ampatzidis, and M., Gianniou, 2008. Evaluation of EGM08 in Greece using GPS and leveling heights, *Proceedings of the IAG International Symposium on Gravity, Geoid and Earth Observation*, Chania, Greece, June 23–27, unpaginated CD-ROM.

Lang, H., and R. Welch, 1999. *ATBD-AST-08 Algorithm Theoretical Basis Document for ASTER Digital Elevation Models. Standard Product AST14 Report*, The Jet Propulsion Laboratory, California Institute of Technology, Los Angeles, California.

Lee, H.-Y., T. Kim, W. Park, and H.-K. Lee, 2003. Extraction of digital elevation models from satellite stereo images through stereo matching based on epipolarity and scene geometry, *Image and Vision Computing*, 21:789–796.

LP DAAC, 2009. Land Processes Distributed Active Archive Center, URL: *http://wist.echo.nasa.gov/api* (last date accessed: 20 November 2010).

MacKinnon, J.G., and H. White, 1985. Some heteroskedasticity consistent covariance matrix estimators with improved finite sample properties, *Journal of Econometrics*, 29:305–325.

Nikolakopoulos, K., E. Kamaratakis, and N. Chrysoulakis, 2006. SRTM vs ASTER elevation products: Comparison for two regions in Crete, Greece, *International Journal of Remote Sensing*, 27:4819–4838.

Pavlis, N.K., S.A. Holmes, S.C. Kenyon, and J.K. Factor, 2008. *An Earth Gravitational Model to Degree 2160: EGM2008*, Presented at the 2008 General Assembly of the European Geosciences Union, Vienna, Austria, 13–18 April.

Quattrochi, D., and M. Goodchild, 1997. *Scale in Remote Sensing and GIS*, CRC Press, Lewis Publishers, New York.

Rosen, P., M. Eineder, B. Rabus, E. Gurrola, S. Hensley, W. Knöpfle, H. Breit, A. Roth, and M. Werner, 2001. SRTM Mission - Cross Comparison of X and C Band Data Properties, *Proceedings of IGARSS*, Sydney, Australia, unpaginated CD-ROM.

Toutin, Th., R. Chénier, and Y. Carbonneau, 2001. 3D Geometric Modelling of Ikonos Geo Images, *Proceedings of the ISPRS Joint Workshop "High Resolution from Space,"* Hannover, Germany, unpaginated CD-ROM.

Toutin, Th., 2008. ASTER DEMs for geomatic and geoscientific applications: a review, *International Journal of Remote Sensing,* 29: 1855–1875.

Toutin, Th., 2004. Geometric processing of remote sensing images: Models, algorithms and method, *International Journal of Remote Sensing*, 25:1893–1924.

Toutin, Th., 2001. Elevation modelling from satellite VIR data: A review, *International Journal of Remote Sensing,* 22:1097–1125.

Welch, R., T. Jordan, H. Lang, and H. Murakani, 1998. ASTER as a source for topographic data in the late 1990s, *IEEE Transactions on Geosciences and Remote Sensing*, 36:1282–1289.

Werner, M., 2001. Status of the SRTM data processing: When will the world-wide 30 m DTM data be available?, *Geo-Informationssysteme*, Heidelberg: Herbert Wichmann/Hüthig, pp. 6–10.

Yamaguchi, Y., A. Kahle, H. Tsu, T. Kawakami, and M. Pniel, 998. Overview of advanced spaceborne thermal emission and reflection radiometer (ASTER), *IEEE Transactions on Geosciences and Remote Sensing*, 36:1062–1071.

Zhen, X., X. Huang, and L.K. Kwoh, 2001. Extracting DEM from SPOT stereo images, *Proceedings of the 20th Asian Conference on Remote Sensing*, Singapore, unpaginated CD-ROM.

(Received 30 March 2010; accepted 08 July 2010; final version 27 September 2010)